INSTITUTE OF PHYSICS PUBLISHING JOURNAL OF PHYSICS A: MATHEMATICAL AND GENERAL

J. Phys. A: Math. Gen. **39** (2006) 4411–4419 doi:10.1088/0305-4470/39/17/S16

Dense plasmas in astrophysics: from giant planets to neutron stars

G Chabrier[1], **D Saumon**[2] **and A Y Potekhin**[3]

[1] Ecole Normale Supérieure de Lyon, CRAL (UMR 5574 CNRS), France
[2] Los Alamos National Laboratory, NM 87545, USA
[3] Ioffe Physico-Technical Institute, St Petersburg, Russia

Received 14 August 2005, in final form 22 November 2005
Published 7 April 2006
Online at stacks.iop.org/JPhysA/39/4411

Abstract
We briefly examine the properties of the dense plasmas characteristic of the interior of giant planets and of the atmospheres of neutron stars. Special attention is devoted to the equation of state of hydrogen and helium at high density and to the effect of magnetic fields on the properties of dense matter.

PACS numbers: 05.70.−a, 64.10.+h, 96.30.Kf, 96.30.Mh, 97.60.Jd

(Some figures in this article are in colour only in the electronic version)

1. Introduction

An accurate determination of the thermodynamic properties of matter under extreme conditions of temperature and density is required for a correct description of the mechanical and thermal properties of many dense astrophysical bodies, including giant planets, low-mass stars (i.e., stars smaller than the Sun) and so-called compact stars (white dwarfs, brown dwarfs and neutron stars). These objects are composed dominantly of ion–electron plasmas, where ions are strongly correlated and electrons are strongly or partially degenerate: the classical Coulomb coupling parameter $\Gamma_{\rm i} = (Z_{\rm i}e)^2/k_BTa_{\rm i}$ is large and the electron density parameter $r_s = a_{\rm i}/\left(a_0 Z_{\rm i}^{1/3}\right)$ is less than unity (here $a_0 = \hbar^2/(m_e e^2)$ denotes the electronic Bohr radius, $a_{\rm i} = (3/4\pi n_{\rm i})^{1/3}$ the mean inter-ionic distance, $Z_{\rm i}$ the ion charge number, and $n_{\rm i}$ the ion number density). The correct description of the structure and cooling of these astrophysical bodies thus requires the knowledge of the equation of state (EOS) and the transport properties of such dense plasmas. In this short review, we focus on the two extremes of this range of astrophysical objects in terms of matter density: Jovian planets and neutron stars. As will be shown in the next sections, modern experiments and observations provide stringent constraints on the thermodynamic properties of dense matter under the physical conditions characteristic of these objects.

2. The equation of state of hydrogen and the structure of Jovian planets

2.1. Hydrogen pressure dissociation and ionization

Jupiter and Saturn are composed of about 70%–97% by mass of hydrogen and helium. Temperatures and pressures range from $T = 170$ K and $T = 136$ K at the $P = 1$ bar surface, respectively, at the surface, to $T > 8000$ K, $P > 10$ Mbar at the centre. At pressures around $P \sim 1$–3 Mbar, corresponding to about 80% and 60% of Jupiter's and Saturn's radius (measured from the centre), respectively, hydrogen undergoes a transition from an insulating molecular phase to a conducting ionized plasma. The description of this transition, described as the pressure ionization or metallization of hydrogen, has remained a challenging problem since the pioneering work of Wigner and Huntington [1]. Much experimental work has been devoted to this problem, but the results remain somewhat inconclusive. Several high-pressure shock wave experiments have been conducted in order to probe the EOS of deuterium, the isotope of hydrogen, in the regime of pressure ionization. Gas gun shock compression experiments were generally limited to pressures below 1 Mbar [2], probing only the domain of molecular hydrogen. New techniques include laser-driven shock wave experiments [3, 5], pulse-power compression experiments [6] and convergent spherical shock wave experiments [7, 8] and can achieve pressures up to 5 Mbar in fluid deuterium at high temperature, exploring for the first time the regime of pressure dissociation and ionization. These recent experiments give different results at $P \gtrsim 1$ Mbar, however, and this controversy needs to be settled before a robust comparison between experiment and theory can be made in the very domain of hydrogen pressure ionization.

On the theoretical front, a lot of effort has been devoted to describing the pressure ionization of hydrogen. The EOS commonly used for modelling Jovian planet interiors is the Saumon–Chabrier–Van Horn (SCVH) EOS [9–11] which includes a detailed description of the partial ionization regime. This EOS reproduces the Hugoniot data of Nellis *et al* [2] but yields temperatures about 30% higher than the gas reshock data, indicating insufficient D_2 dissociation [12]. A slightly revised version [13] recovers the gas gun reshock temperature data as well as the laser-driven shock wave results [3], with a maximum compression factor of $\rho/\rho_0 \simeq 6$, where $\rho_0 = 0.17$ g cm^{-3} is the initial density of liquid deuterium at 20 K. On the other hand, the earlier SESAME EOS [14], based on a similar formalism, predicts a smaller compression factor, with $\rho/\rho_0 \simeq 4$, in general agreement with all the other recent shock wave experiments. *Ab initio* approaches for the description of dense hydrogen include path integral Monte Carlo (PIMC) [15–17] and quantum molecular dynamics (QMD) simulations. The latter combine molecular dynamics (MD) and density functional theory (DFT) to take into account the quantum nature of the electrons [18–21]. The relevance of earlier MD-DFT calculations was questioned on the basis that these simulations were unable to reproduce data from gas gun experiments [18]. This problem has been solved with more accurate simulations [19–21]. Although an *ab initio* approach is more satisfactory than the phenomenological approach based on effective potentials, in practice these simulations also rely on approximations, such as the handling of the so-called sign problem for the antisymmetrization of the fermion wave functions, or the calculation of the electron functional density itself (in particular the exchange and correlation effects), or the use of effective pseudo-potentials of restricted validity, addition to finite size effects. Moreover, these simulations are too computationally intensive for the calculation of an EOS covering several orders of magnitude in density and temperature, as necessary for the description of the structure and evolution of astrophysical bodies.

Figure 1 compares experimental and theoretical Hugoniots in the P–ρ and P–T planes. The disagreement between the laser-driven experiments and the other techniques is illustrated in the P–ρ diagram. Whereas the SCVH EOS achieves a maximum compression similar to the

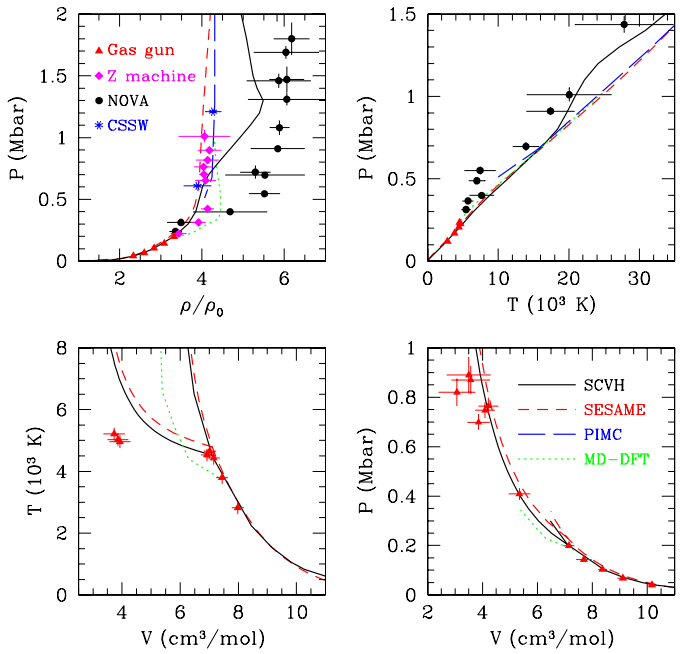

Figure 1. Experimental shock (P, ρ, T) data and theoretical Hugoniots of deuterium. Sources of data are gas gun *et al* [2, 12], Z machine [6], NOVA [3, 4] and CSSW [7, 23]. Curves show Hugoniots computed from the EOSs of SCVH [11], SESAME [14], PIMC [15] and MD-DFT [20].

laser-driven data, all the other models predict compression factors in the P–ρ plane in agreement with the more recent data. The MD-DFT results, however, predict temperatures for the second shock significantly larger than the experimental results [12]. Even though the experimental double-shock temperature may be underestimated due to unquantified thermal conduction into the window upon shock reflection, and thus represents a lower limit on the reshock temperatures, the disagreement in the T–V plane is significant. As noted previously, the degree of molecular dissociation has a significant influence on the thermodynamic properties of the fluid and insufficient dissociation in the simulations may result in overestimates of the temperature. It has been suggested that the LDA/GGA approximations used in MD-DFT underestimate the dissociation energy of D_2 [22]. This would lead to even less dissociation. The fact that compression along the experimental Hugoniot remains small thus suggests compensating effects in the case of hydrogen. More recent, improved simulations [21], however, seem to partly solve this discrepancy and to produce reshock temperatures in better agreement with the experimental results. Peak compression in the modern MD-DFT simulations occurs in the ∼0.2–0.5 Mbar range around a dissociation fraction of ∼50%.

The differences in the behaviour of hydrogen at high density and temperature illustrated by the various results displayed in figure 1 bear important consequences for the structure and evolution of our Jovian planets. These differences must be correctly understood before the description of hydrogen pressure dissociation and ionization stands on firm grounds. As noted by Boriskov *et al* [23], all the recent experiments agree quite well in terms of the shock speed u_s versus the particle velocity u_p, almost within their respective error bars. Error bars and differences in (u_s, u_p) are amplified in a P–ρ diagram by a factor of $(\rho/\rho_0 - 1)$. These are challenging experiments as the differences seen in panel 1 of figure 1 arise from differences in u_s and u_p of less than 3%.

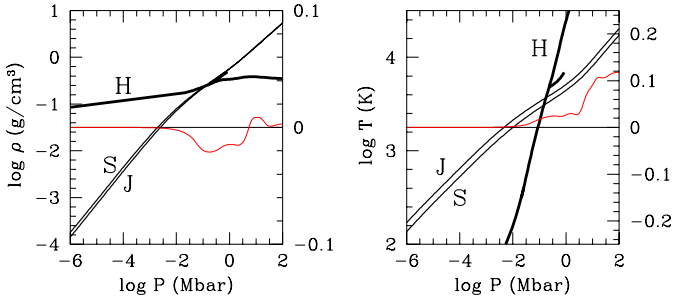

Figure 2. Adiabats for hydrogen in P–ρ and P–T planes. The curves labelled 'S' and 'J' show the SCVH-interpolated EOS adiabats of Saturn and Jupiter, determined by $T = 136$ K and $T = 170$ K at $P = 1$ bar, respectively. The first and second-shock Hugoniots calculated with the SESAME EOS are shown by the heavy solid line labelled 'H'. The light solid curve (right-hand scale) shows the *difference* between Jupiter adiabats calculated with the SESAME EOS relative to the SCVH-interpolated EOS.

2.2. The interiors of Jupiter and Saturn

The rapid rotation of Jovian planets induces a non-spherical gravitational field that can be expanded in Legendre polynomials $P_n(\cos\theta)$:

$$V(r,\theta) = -\frac{GM}{r}\left[1 - \sum_{n=1}^{\infty}\left(\frac{R_{\rm eq}}{r}\right)^n J_n P_n(\cos\theta)\right], \tag{1}$$

where M and $R_{\rm eq}$ denote, respectively, the planet mass and equatorial radius, and the J_n are the gravitational moments:

$$J_n = -\frac{1}{M R_{\rm eq}^n}\int_V r'^n P_n(\cos\theta)\rho(r',\theta)\,{\rm d}^3 r'. \tag{2}$$

Because of north-south symmetry, the moments of odd order are null. The first three non-vanishing moments, J_2, J_4 and J_6, have been measured with high accuracy for both planets during spacecraft fly-by missions. Combined with the planet mass, radius and rotation period, these provide integral constraints on the density profile of the planet, $\rho(r,\theta)$, to be compared with the corresponding values from a structure model obtained for a self-gravitating and rotating fluid body in hydrostatic equilibrium. The EOS provides the $P(\rho)$ relation needed to close the system of equations. The structure of the H/He envelopes of giant planets is fixed by the specific entropy determined from observations at their surface. The very high efficiency of convection in the interior of these objects leads to nearly adiabatic interior profiles. The structure of the planet is thus determined by the choice of the hydrogen EOS and to a lesser extent by the helium EOS used in the models. A detailed study of the influence of the EOS of hydrogen on the structure and evolution of Jupiter and Saturn has been conducted recently [24]. Fortunately, some shock wave experiments overlap Jupiter's and Saturn's adiabats. Figure 2 displays Jupiter (J) and Saturn (S) adiabats for hydrogen calculated with the SCVH EOS and the first and second shock Hugoniots calculated with the SESAME EOS and illustrates the *relative differences* in density between Jupiter adiabats computed with these two EOSs. As demonstrated by Saumon and Guillot [24], the small ($\leqslant 5\%$) difference on the (P,ρ) relation along the adiabat between the two EOSs, representative of the two sets of experimental results, is large enough to affect appreciably the interior structure of the models. Note that the SESAME D_2 Hugoniot at low density is somewhat stiffer than the gas gun experiments [2] and does not recover the ideal D_2 gas entropy at low temperature and density. No model

of Jupiter could be obtained with this EOS [24]. A slightly modified SESAME EOS, which does recover the H_2 entropy at low temperature and density, yields Jupiter models with a very small core mass, $M_{\rm core} \sim 1$ $M_\oplus$ ($M_\oplus$ is the mass of the Earth) and a mass $M_Z \sim 33$ $M_\oplus$ of heavy elements ($Z > 2$) mixed in the H/He envelope. The SCVH EOS yields models with $M_{\rm core} = 0$–4 $M_\oplus$ and $M_Z \sim 15$–26 $M_\oplus$. Models of Saturn are less sensitive to the EOS differences, since only ∼70% of its mass lies at $P > 1$ Mbar, compared to 91% for Jupiter. Models computed with the SCVH and the modified SESAME EOS have $M_{\rm core} = 10$–21 $M_\oplus$ and $M_Z = 1$–6 $M_\oplus$ and 4–8 $M_\oplus$, respectively. As seen in figure 2, the temperature along the adiabat is more sensitive to the choice of the EOS. This affects the thermal energy content of the planet and thus its cooling rate and evolution. Equations of state which are adjusted to fit the deuterium reshock temperature measurements [25] lead to models that take ∼3 Gyr for Jupiter to cool to its present state. Even when considering uncertainties in the models, or considering the possibility of a H/He phase separation, such a short cooling age is unlikely to be reconciled with the age of the solar system. This astrophysical constraint suggests that the reshock temperature data are too low.

2.3. Helium equation of state and the plasma phase transition

The planet interior models are also affected, to a lesser extent, by the uncertainties of the helium EOS. A model EOS for helium at high density, covering the regime of pressure ionization, has been developed recently by Winisdoerffer and Chabrier [26]. This EOS, based on effective interaction potentials between He, He^+, He^{++} and e^- species, reproduces adequately experimental Hugoniot and sound speed measurements up to ∼1 Mbar. In this model, pressure ionization is predicted to occur directly from He to He^{++}. Because of the uncertainties in the treatment of the interactions at high density, however, the predicted ionization density ranges from a few to ∼10 g cm^{-3}. Comparison of the model predictions with available measurements of electrical conductivity of helium at high density [27, 28] is under way.

The pressure ionization and metallization of hydrogen have been predicted to occur through a first-order phase transition, the so-called plasma phase transition (PPT) [1, 29–31, 10, 42]. Nearly all of these PPT calculations are based on chemical EOS models. Such models are based on a Helmholtz free energy that includes contributions from (1) neutral particles (atoms and molecules), (2) a fully ionized plasma and (3) usually a coupling between the two. It is well known that realistic fully ionized plasma models become thermodynamically unstable at low temperatures and moderate densities. This is analogous to the behaviour of expanded metals at $T = 0$ that display a region where $\mathrm{d}P/\mathrm{d}\rho < 0$ and even $P < 0$ [32]. This behaviour of the fully ionized plasma model is formally a first-order phase transition and reflects the formation of bound states in the real system. In other words, the chemical models have a first-order phase transition built in from the onset, and this phase transition coincides, not surprisingly, with the regime of pressure ionization. This represents a common flaw in this type of models and it follows that their prediction of a PPT in hydrogen is not credible. This is further supported by a detailed study of two of these models [10, 42]. On the other hand, recent *ab initio* simulations find a sharp ($6 \pm 2\%$) volume discontinuity at constant pressure [21, 33] or $\mathrm{d}P/\mathrm{d}T < 0$ at constant volume [43–45], a feature consistent with the existence of a first-order phase transition. At the same time, the pair correlation function exhibits a drastic change from a molecular to an atomic state with a metallic character (finite density of electronic states at the Fermi level). These transitions are found to occur in the ∼0.5–1.25 Mbar and ∼1500–3000 K temperature range. While these results are suggestive, a systematic exploration of this part of the phase diagram remains to be done. Note that a

first-order structural transition for H_2 at $T = 0$ is predicted to occur at a pressure $P \gtrsim 4.0$ Mbar, from DFT calculations based on *exact* exchange calculations [22]. There is so far no published experimental evidence for the PPT but it cannot yet be ruled out. Given the difficulty of modelling this region of the phase diagram of hydrogen, only experiments can ultimately establish whether a PPT exists or not.

3. Dense matter in strong magnetic fields: neutron star structure and cooling

Neutron stars (NS) consist of a core of nucleons surrounded by an envelope of nuclei and electrons forming a Coulomb plasma. Cooling rates of these stars are determined by the heat capacity and neutrino emission processes in their cores and by heat transport in the envelopes. For the neutrino emission, most important are the so-called direct Urca (Durca) processes (beta-decay and beta-capture) and modified Urca (Murca) processes (the same but with participation of an additional nucleon, which helps to fulfil momentum conservation). The Murca processes are less efficient, but they work in every sufficiently hot NS. In contrast, the most efficient Durca processes operate only if the proton fraction in the core is large enough (otherwise the momentum conservation condition for degenerate nucleons cannot be satisfied). Some models of nuclear matter predict that a NS with relatively high mass should have a sufficient proton fraction at the stellar centre for the Durca processes to occur. Such stars should cool faster, which opens a possibility of testing the EOS of superdense matter through observations. The cooling rates are also strongly affected by nucleon superfluidity (see [34] for review and references).

Most NSs have magnetic fields $B \sim 10^{11}$–10^{13} G, whereas some (so-called magnetars) are thought to have fields as high as $\sim 10^{14}$–10^{15} G. The photosphere of a NS is characterized by temperatures $T_s \simeq 10^5$–10^7 K (depending on the age t and mass M of the star) and densities $\rho \simeq 10^{-2}$–10^4 g cm^{-3} (depending on T and B). Traditionally the NS crust is assumed to be composed of iron. However, the outer layers, including the atmosphere, can be composed of light elements (H, He, C) accreted on top of the iron layer. Therefore the determination of the temperature profiles and emitted spectra of NSs requires an accurate description of the formation of bound states and pressure ionization of these elements in a strong magnetic field.

The quantum-mechanical properties of free charged particles and bound species (hydrogen atoms and molecules) are strongly modified by the magnetic field, which thereby affects the thermodynamic properties of the plasma [35, 36]. The transverse motion of electrons in a magnetic field is quantized into Landau levels. The energy of the nth Landau level of the electron (without the rest energy) is $m_e c^2(\sqrt{1+2bn}-1)$, which becomes $\hbar\omega_c n$ in the non-relativistic limit, where $\hbar\omega_c = \hbar eB/m_e c = 11.577 B_{12}$ keV, is the electron cyclotron energy, $b = \hbar\omega_c/m_e c^2 = B_{12}/44.14$ is the field strength in the relativistic units, and $B_{12} = B/(10^{12}\ \mathrm{G})$ is a typical magnetic-field scale for NS conditions. The atomic unit for the magnetic-field strength is set by $\hbar\omega_c = e^2/a_0$, i.e., $B_0 = (m_e c/\hbar e) \times (e^2/a_0) = 2.35 \times 10^9$ G. It is convenient to define a dimensionless magnetic-field strength $\gamma = B/B_0 = b/\alpha_f^2$, where α_f is the fine structure constant.

For $\gamma \gg 1$, as encountered in NSs, the ground-state atomic and molecular binding energies increase as $\sim \ln^2 \gamma$. The H atom in a strong magnetic field is compressed in the transverse directions to the radius $\sim a_m$, where

$$a_m = (\hbar c/eB)^{1/2} = \gamma^{-1/2} a_0 = 2.56 \times 10^{-10} B_{12}^{-1/2}\ \mathrm{cm} \tag{3}$$

is the quantum magnetic length, which becomes the natural length unit. The increase of binding energies and decrease of sizes lead to a significant increase of the fraction of non-ionized atoms in the plasma at the photospheric densities (which are higher for stronger magnetic

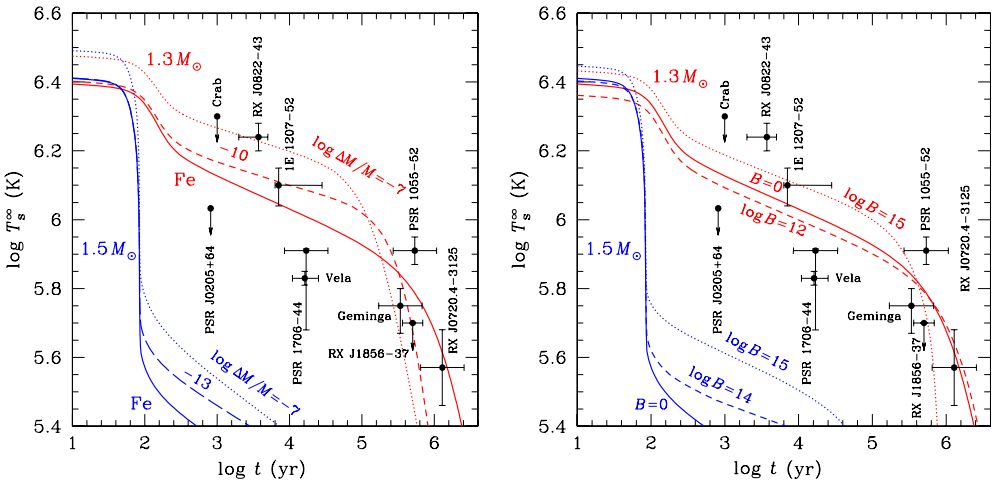

Figure 3. Effective surface temperature (as seen by a distant observer, T_s^∞) versus NS age t for assumed NS mass $M = 1.3$ and 1.5 solar masses. The dots with error bars show estimates of NS ages and effective temperatures from various observations; the dots with arrows indicate observational upper limits. Left: cooling of NSs with different relative masses $\Delta M/M$ of accreted (H–He–C) matter (values of $\log \Delta M/M$ are indicated near the curves). Solid curves refer to non-accreted (Fe) iron envelope of the star. Right: cooling of NSs with iron envelope for different magnetic field strengths ($\log B$ in Gauss).

fields). For example, at $T = 10^6$ K and $B = 10^{13}$ G, the typical density is $\rho \sim 1$ g cm^{-3}, and there are $>1\%$ of atoms in the H atmosphere. Because of the alignment of the electron spins antiparallel to the field, two atoms in their ground state ($m = 0$) do not bind together, because of the Pauli exclusion principle. One of the two H atoms has to be excited in the $m = -1$ state to form the ground state of the H_2 molecule [36]. Another important effect is that thermal motion of atoms across the field strongly modifies their binding energies and radiative transition rates. As shown in [37–39], the allowance for partial ionization and thermal motion is crucial for neutron-star atmosphere modelling.

As long as $T \ll \hbar\omega_c/k_B = 1.343 \times 10^8 B_{12}$ K and $\rho \ll \rho_B \approx 7.1 \times 10^3 B_{12}^{3/2}$ g cm^{-3}, the electron cyclotron energy $\hbar\omega_c$ exceeds both the thermal energy $k_B T$ and the electron Fermi energy $k_B T_F$, so that the field is *strongly quantizing* (e.g., [35]). In this case, typical for the NS photospheres, the electron spins are aligned antiparallel to the field. The electron Fermi energy decreases; therefore the onset of degeneracy is shifted to higher densities (slightly below ρ_B). Proton motion is also quantized by the magnetic field, but the corresponding cyclotron energy is much smaller, $\hbar\omega_{cp} = \hbar\omega_c m_e/m_p$.

A model which describes the thermodynamics of an interacting (H_2, H, H^+, e^-) plasma in a strong magnetic field was constructed in [37]. On the base of this model, the EOS for magnetized H atmospheres of NSs, as well as their opacities, were explored and tabulated in [38, 39].

Landau quantization of electron orbits affects not only the EOS and the radiative opacities, but also the heat conduction in the surface layers (see [35] and references therein). The EOS of strongly magnetized, partially ionized hydrogen plasma as well as the electron conductivities and radiative opacities in neutron star magnetized envelopes were used in [40] to calculate the thermal structure and cooling of superfluid NSs with accreted envelopes in the presence of strong dipole magnetic fields. In [40] (see also [41] and references therein), the effect of

neutron superfluidity in the NS inner crust was also examined. The account of the effects of accreted matter, magnetic field and neutron superfluidity alters the NS cooling significantly.

Figure 3 displays theoretical cooling curves of NSs with (lower curves, $M = 1.5\ M_\odot$) or without (upper curves, $M = 1.3\ M_\odot$) Durca processes in the core, with or without accreted envelopes, and with magnetic field of different strengths, compared to the estimates of the effective temperature obtained from observations (see [34] for references). As seen in the figure, the presence of a light-element (accreted) envelope increases T_s at the early cooling stage ($t \lesssim 10^5$ yr), and as a result the thermal energy becomes exhausted sooner. The magnetar-like magnetic field $B \gtrsim 10^{14}$ G acts in a similar way, whereas a weaker field almost does not affect the cooling.

For simplicity, in figure 3 we neglect the effects of superfluidity. Their discussion can be found in [34, 40, 41].

4. Conclusions

In this brief review, we considered the description of the thermodynamic properties of dense Coulomb matter in two specific astrophysical contexts, Jovian planets and neutron stars. The description of the pressure ionization of hydrogen and other elements, as well as the presence of strong magnetic fields, plays an important role in determining the mechanical and thermal properties and the evolution of these objects. Models including these complex effects can successfully explain a variety of observations. On the other hand, modern experiments and/or observations can enable us to discriminate between various EOS models in planet interiors and lead to a better determination of masses of accreted envelopes, surface magnetic fields and eventually the EOS of superdense matter in neutron stars.

Acknowledgments

We thank D G Yakovlev for providing us with his compilation of observational data and performing cooling calculations with our physics input for figure 3. The work of GC was partially supported by the CNRS French–Russian grant PICS 3202. The work of AYP was partially supported by the RLSS grant 1115.2003.2 and the RFBR grants 05-02-16245, 03-07-90200 and 05-02-22003. The work of DS was supported in part by the United States Department of Energy under contract W-7405-ENG-36.

References

[1] Wigner E and Huntington H B 1935 *J. Chem. Phys.* **3** 764
[2] Nellis W J, Mitchell A C, van Thiel M, Devine G J, Trainor R J and Brown N 1983 *J. Chem. Phys.* **79** 1480
[3] Collins G W *et al* 1998 *Science* **281** 1178
[4] Collins G W *et al* 2001 *Phys. Rev. Lett.* **87** 165504
[5] Mostovych A N, Chan Y, Lehecha T, Schmitt A and Sethan J D 2000 *Phys. Rev. Lett.* **85** 3870
[6] Knudson M D, Hanson D L, Bailey J E, Hall C A, Asay J R and Deeney C 2004 *Phys. Rev.* B **69** 144209
[7] Belov S I *et al* 2002 *JETP Lett.* **76** 433
[8] Boriskov G V, Bykov A I, Ilkaev R I, Selemir V D, Simakov G V, Trunin R F, Urlin V D, Fortov V E and Shuikin A N 2003 *Dokl. Phys.* **48** 553
[9] Saumon D and Chabrier G 1991 *Phys. Rev.* A **44** 5122
[10] Saumon D and Chabrier G 1992 *Phys. Rev.* A **46** 2084
[11] Saumon D, Chabrier G and Van Horn H M 1995 *Astrophys. J. Suppl. Ser.* **99** 713
[12] Holmes N C, Ross M and Nellis W J 1995 *Phys. Rev.* B **52** 15835
[13] Saumon D, Chabrier G, Xu and Wagner 2000 *High Press. Res.* **16** 331
[14] Kerley G 1972 *Los Alamos Laboratory Report* LA-4476

[15] Militzer B and Ceperley D M 2000 *Phys. Rev. Lett.* **85** 1890
[16] Militzer B, Ceperley D M, Kress J D, Johnson J D, Collins L A and Mazevet S 2001 *Phys. Rev. Lett.* **87** 275502
[17] Bezkrovniy V, Filinov V S, Kremp D, Bonitz M, Schlanges M, Kraeft W D, Levashov P R and Fortov V E 2004 *Phys. Rev.* E **70** 057401
[18] Lenosky T, Bickham S R, Kress J D and Collins L A 2000 *Phys. Rev.* B **61** 1
[19] Bagnier S, Blottiau P and Clérouin J 2001 *Phys. Rev.* E **63** 015301
[20] Desjarlais M P 2003 *Phys. Rev.* B **68** 064204
[21] Bonev S A, Militzer B and Galli G 2004 *Phys. Rev.* B **69** 014101
[22] Städele M and Martin R M 2000 *Phys. Rev. Lett.* **84** 6070
[23] Boriskov G V, Bykov A I, Ilkaev R I, Selemir V D, Simakov G V, Trunin R F, Urlin V D, Shuikin A N and Nellis W J 2005 *Phys. Rev.* B **71** 092104
[24] Saumon D and Guillot T 2004 *Astrophys. J.* **609** 1170
[25] Ross M 1998 *Phys. Rev.* B **58** 669
Ross M 1999 *Phys. Rev.* B **60** 6923 (erratum)
[26] Winisdoerffer C and Chabrier G 2005 *Phys. Rev.* E **71** 026402
[27] Ternovoi V Ya *et al* 2001 *Shock Compression of Condensed Matter* ed M Furnish, N Thadhani and Y Horie (New York: AIP) p 107
[28] Fortov V E *et al* 2003 *JETP* **97** 259
[29] Norman G E and Starostin A N 1968 *High Temp.* **6** 394
[30] Ebeling W and Richert W 1985 *Phys. Lett.* A **108** 80
[31] Saumon D and Chabrier G 1989 *Phys. Rev. Lett.* **62** 2397
[32] Pines D and Nozières P 1966 *Theory of Quantum Fluids* (New York: Benjamin)
[33] Scandalo S 2003 *Proc. Natl. Acad. Sci. USA* **100** 3051
[34] Yakovlev D G and Pethick C 2004 *Annu. Rev. Astron. Astrophys.* **42** 169
[35] Ventura J and Potekhin A Y 2001 *The Neutron Star–Black Hole Connection (NATO ASI Series C* vol 567*)* ed C Kouveliotou, J Ventura and E van den Heuvel (Dordrecht: Kluwer) p 393
[36] Lai D 2001 *Rev. Mod. Phys.* **73** 629
[37] Potekhin A Y, Chabrier G and Shibanov Yu A 1999 *Phys. Rev.* E **60** 2193
[38] Potekhin A Y and Chabrier G 2003 *Astrophys. J.* **585** 955
[39] Potekhin A Y and Chabrier G 2004 *Astrophys. J.* **600** 317
[40] Potekhin A Y, Yakovlev D G, Chabrier G and Gnedin O Y 2003 *Astrophys. J.* **594** 404
[41] Yakovlev D G, Gnedin O Y, Gusakov M E, Kaminker A D, Levenfish K P and Potekhin A Y 2005 *Nucl. Phys.* A **752** 590
[42] Kitamura H and Ichimaru S 1998 *J. Phys. Soc. Japan* **67** 950
[43] Magro W R, Ceperley D M, Pierleoni C and Bernu B 1996 *Phys. Rev. Lett.* **76** 1240
[44] Bagnier S, Blottiau P and Clérouin J 2000 *Phys. Rev.* E **63** 015301
[45] Filinov V S, Bonitz M, Fortov V E, Ebeling W, Levashov P and Schlanges M 2004 *Contrib. Plasma Phys.* **44** 388